Available online at www.sciencedirect.com
ScienceDirect
Journal of Computational Physics 219 (2006) 532–552
JOURNAL OF COMPUTATIONAL PHYSICS
www.elsevier.com/locate/jcp

Density distribution for a dense hard-sphere gas in micro/nano-channels: Analytical and simulation results

S.V. Nedea [a,*], A.J.H. Frijns [a], A.A. van Steenhoven [a], A.P.J. Jansen [b], A.J. Markvoort [c], P.A.J. Hilbers [c]

[a] *Department of Mechanical Engineering, Eindhoven University of Technology, P.O. Box 513, 5600MB Eindhoven, The Netherlands*
[b] *Department of Chemical Engineering, Eindhoven University of Technology, P.O. Box 513, 5600MB Eindhoven, The Netherlands*
[c] *Department of Biomedical Engineering, Eindhoven University of Technology, P.O. Box 513, 5600MB Eindhoven, The Netherlands*

Received 7 July 2005; received in revised form 2 February 2006; accepted 3 April 2006
Available online 2 June 2006

Abstract

We study the properties of a hard-sphere dense gas near the hard walls of micro and nano-channels. Analytical techniques, Monte Carlo (MC) methods and molecular dynamics (MD) simulation methods have been used to characterize the influence of the characteristic parameters such as number density, reduced density, width of the system and molecular diameter, on the equilibrium properties of the gas near the hard walls of micro and nano-channels. A mathematical model has been developed to characterize the density oscillations as the result of packing of molecules in case of a dense gas near the micro and nano-channels walls. The height and the position of the density oscillation peaks near the wall are characterized. These results are also confirmed by the MD and MC simulation results.

Comparisons between MD and MC simulation results for particles having different diameter are also presented. For the same size of the particles and moderately dense gas, MC and MD results are similar, differences in the density profiles being limited only to the oscillatory region. For different particle sizes, MD and MC results are limited to a short distance near the wall for long size systems and moderately dense fluids. The effect of the boundary (particle size) on the simulation results is found to increase with η (reduced density) and it is very small in case of a dilute gas. For small η and small particle size (R) relative to the width of the system L, the height of the oscillation peaks is slowly increasing with R/L, and for high densities is always decreasing with R/L. The position of these peaks depends only on the size of the particles and when R is much smaller than L, it shows a small dependence on L. The deviations in the oscillatory region for the pure MC simulation results compared to pure MD simulation results are quantified, and more efficient hybrid MC–MD simulations are performed to reduce these deviations.

Keywords: Micro fluidics; Solid–gas interface; Analytical modeling; Hard-sphere gas behaviour; Micro and nano-channels; Particle simulation methods; Monte Carlo and molecular dynamics; Hybrid simulations

* Corresponding author. Tel.: +31 4024 75 410; fax: +31 4024 33 445.
E-mail address: S.V.Nedea@tue.nl (S.V. Nedea).

0021-9991/$ - see front matter
doi:10.1016/j.jcp.2006.04.002

1. Introduction

While miniaturizing electronic components heat management becomes a very important problem, especially since the power consumption increases with a factor of 10 every 6 years [19]. For ensuring optimal performance and lifetime, new solutions for the cooling of these components will be required. Since local heat sources appear during operation of these devices, local cooling is wanted. Single and two-phase forced convective flows in microchannels become more and more a promising technique for the cooling of electronic components.

The microchannel cooling represents a compact and efficient way of transferring heat from a power source to a fluid. Macroscopic models for heat transfer are not sufficient to describe this cooling mechanism in microstructures. The validity of the continuum approach has been identified with the validity of the Navier Stokes equations [4]. This requires that the Knudson number ($Kn = \lambda/L$, where λ is the mean free path and L the physical length of the system) should be small compared to unity, the limit being $Kn = 0.1$. When the characteristic size of the device decreases or when the flow is more rarefied ($Kn > 0.1$), the continuum flow model is no longer valid and must be replaced by another model. The governing equations of the flow model must change from the Navier Stokes equations to the Boltzmann equation [4,8,7], which involves the molecular velocities instead of the macroscopic quantities. To solve this integro-differential equation for the velocity distribution function using conventional finite element or finite difference methods is difficult since the number of independent variables include both those of physical space and those of the velocity space. The alternative is to use a molecular model, where the volume is filled with a large number of discrete molecules and to apply different particle simulation methods to solve the Boltzmann equation taking into account the molecular structure of gases.

These particle simulation methods are molecular dynamics (MD) [6] and direct simulation Monte Carlo method (DSMC) [1,2,4,10]. In MD, the time evolution of a set of interacting molecules is followed exactly. Molecules move and collide according to the forces they exert on each other. In DSMC, movements and collisions of particles occur between large particles concentrating a cluster of real molecules. Collisions are generated stochastically with scattering rates and post-collision velocity distributions determined from the kinetic theory.

MD simulations are able to simulate small-scale effects near the solid wall and near the boundaries of phase transitions accurately. However, because all the pair interactions between all particles have to be calculated, the MD method is too time consuming for the number of particles needed to simulate a dense gas dynamics in micro and nano-channels. For simulating a dense gas flow in a microchannel, the MD method becomes very time consuming.

For a dense gas the governing equation of the flow model is an extension of the Boltzmann equation, called Enskog equation [5,20]. Different MC particle simulation methods have been proposed to solve this equation. The first method described by Garcia [1,2] is an attempt to bring into DSMC [4] the spatial correlations which are absent in an ideal gas. This method encounters problems with boundary conditions as walls are introduced. A particle method for the numerical solution of the Enskog equation has been presented by Montanero and Santos [11,12] extending the scheme originally proposed by Nanbu [13] for the Boltzmann equation. The method correctly reproduced the transport properties of the Enskog gas, but inherited from the original Nanbu scheme the feature of conserving momentum and energy only in a statistical way and not in a single collision. The particle method proposed by Frezzotti [8] constructed for the Enskog equation in the spirit of the DSMC method exactly conserves momentum and energy. We use this method for our MC results.

As through evaporation we can dissipate large amounts of heat, improving in this way the microchannel cooling process, we need to investigate the small-scale effects that appear near the walls, as these phase boundaries effects become very important for the heat transfer properties. In [7,8], from the simulation of a dense hard-sphere gas confined between two parallel smooth walls using this method, density oscillations were reported near the walls. The near-surface density oscillations have been already reported in the literature for some time [21].

These density oscillations occur over a scale of the order of the molecular diameter and the number and the height of these peaks were reported to depend on the density. The comparisons with the accurate MD simulations show that for high densities, differences between MD and MC were limited only to the oscillatory region. MC results are not accurate in the region next to the wall, specially for a dense flow gas, and MD are very accurate but computationally very expensive.

A hybrid method [9,14] combining MC for particles in the middle of the system and MD for oscillatory region next to the hard walls can be used for our simulation results in order to get fast simulations and also accurate results for the interaction with the wall. Thus, we need first to characterize how the oscillations depend on the system parameters such as number density, width of the channel and molecular diameter. For certain properties of the gas we can thus determine the region near the wall where deviations between results using MD and MC occur and apply the hybrid method, by doing MD approach in this region in order to get accurate results and MC in the bulk. In MC particle simulation methods, usually clusters of molecules are concentrated in one simulating particle ending then in simulation of large simulating particles. The effect of particle size on the simulation results in the middle of the channel for different sizes of the system, and the influence on the region of oscillations is also to be investigated. With these results, efficient and accurate hybrid MD–MC simulations can be performed in order to study the properties at the interface between the gas and the wall for a very dense gas. The dependence of the deviations for high densities, considering different simulation domains in the hybrid MD–MC method is to be analyzed.

In this paper, for the simulation of a dense gas in a microchannel, analytical techniques, Monte Carlo methods and molecular dynamics simulation methods have been used to characterize the influence of the characteristic parameters such as number density, reduced density (η), width of the system and molecular diameter on the equilibrium properties of the gas near the hard walls of the microchannel. This information will be later used to optimize our hybrid MD–MC simulations depending on system parameters. First, we describe the simulation methods used giving the theoretical background for our MD, MC and hybrid MD–MC simulations. Comparisons between MD and MC results for particle of different sizes are presented. We come then with a one-dimensional mathematical model to explain the packing of molecules near the wall. Results of the calculations by testing of the mathematical model are presented. MC simulation results are presented describing the dependence of the oscillations peaks on system parameters. Depending on this analysis on the dependence of the oscillation region on system parameters, we apply a hybrid simulation method, performing MD in the estimated oscillation region and MC for the bulk properties. Finally, the deviations of the hybrid simulation results, considering different lengths of the MD and MC simulation domains are quantified.

2. Theory

We give the theoretical background for the numerical and simulation results. First, we specify our physical model and then we describe the simulation methods used for our system, i.e. MC, MD and hybrid MD–MC simulation methods.

2.1. The physical model

Our model to study the one-dimensional heat flow in a microchannel consists of two parallel infinite plates at a distance L apart from each other and of gas molecules confined between these two walls. An example is shown in Fig. 1. Both plates have their own temperature, T_1 and T_2, respectively, where this temperature is uniform on the plate surface and constant in time. The gas consists of spherical particles of diameter a and mass m, at temperature T. The density of the gas can be expressed as n, being the number of particles per unit of volume, or using a reduced density η, which also takes the particle sizes into account and is related to the number density as $\eta = \pi n a^3/6$ [8]. The mean free path of the gas particles is related to this reduced density. For a relatively dense gas with $\eta \approx 0.1$, the mean free path $\lambda(\lambda = 1/(\sqrt{2}\pi a^2 n Y(\eta)))$ and the molecular diameter a have the same order of magnitude. The Y factor is the pair correlation function at contact and its dependence on η is introduced in the following section. The distance L between the plates, in the x-direction, is always such that both plates are only a few mean free paths apart.

2.2. Particle simulation methods

We are looking at density profiles of a dense gas in equilibrium near the hard wall of micro and nano-channel. We study these profiles by means of particle simulations methods like MC, MD, and hybrid MD–MC.

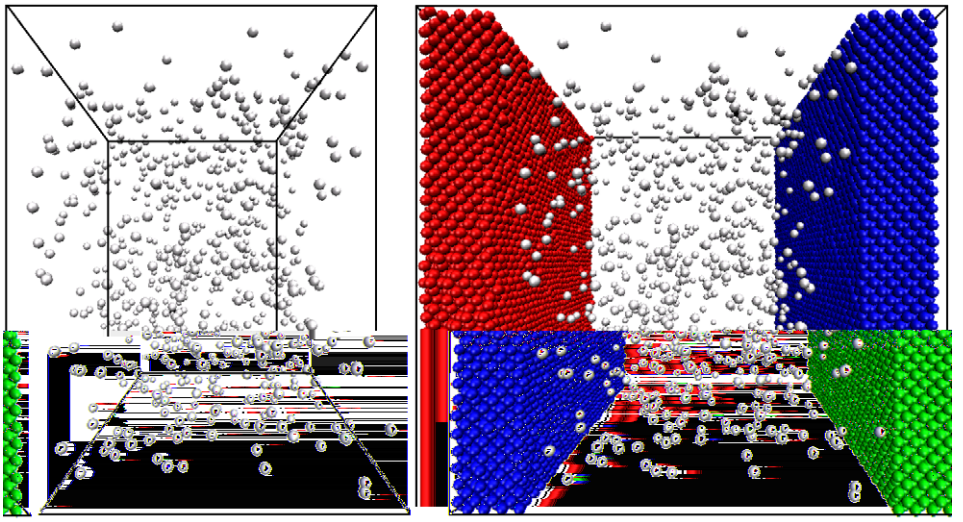

Fig. 1. The model of a microchannel consists of a two parallel infinite plates at distance L apart from each other, and of a gas molecules confined between these plates. Depending on the simulation method, the walls can be modelled: (a) using boundary conditions, or (b) explicitly.

2.3. Monte Carlo methods

The first simulation method used is an extended version of the direct simulation Monte Carlo method. The method is based on the Enskog kinetic equation [5]. This Enskog equation is an extension of the Boltzmann equation to dense fluids and has the form

$$\frac{\partial F}{\partial t} + \xi \circ \nabla F = J_{\mathrm{E}}(F, F), \tag{1}$$

where $F(x,\xi,t)$ is the one-particle distribution function of the molecular velocity ξ. The collision integral $J_{\mathrm{E}}(F,F)$ keeps the same binary structure of the corresponding Boltzmann term, but the colliding molecules occupy different positions in space and the collision frequency is modified by the factor Y which plays the role of an approximate pair correlation function [7,8]. In the standard Enskog theory (SET) [20] of the hard-sphere fluid, the representation of the pair distribution function is the product of two one-particle distribution function times the pair correlation function $Y(n)$ in a state of uniform equilibrium evaluated at the contact point. In equilibrium, relation between Y and the equation of state (EOS) is as given by Resibois and DeLeener [15]:

$$Y(n) = \frac{1}{nb}\left(\frac{p}{nkT} - 1\right), \tag{2}$$

where p being the pressure and $b = 2\pi a^3/3$. The equation of state of the hard-sphere fluid cannot be given in a closed form, but various approximate expressions have been proposed. Carnahan and Starling [16] found a clever way to represent the hard-sphere gas EOS by a simple expression from which an approximate Y can be obtained. The approximation by Carnahan and Starling has been used here:

$$\frac{1 + \eta + \eta^2 - \eta^3}{(1-\eta)^3}, \tag{3}$$

where $\eta = \pi a^3 n/6$, yielding the Y function having the form:

$$Y(\eta) = \frac{1}{2}\frac{2-\eta}{(1-\eta)^3}. \tag{4}$$

The expression for the mean free path given in the previous section, comes from the Enskog's collision term, which, in uniform distribution, takes the same form as Boltzmann's collision term [17,18], except for the Y factor.

The important macroscopic quantity that we are computing in our MC simulations is the number density. In terms of the one-particle distribution function F, this property can be written as it follows:

Number density

$$n(x) = \int F(x, \xi)\, \mathrm{d}\xi. \tag{5}$$

The Enskog equation can be solved numerically by means of a particle simulation method, as proposed by Frezzotti in 1997 [7,8], to study the one-dimensional steady heat flow in a dense hard-sphere gas. In this particle simulation method, the molecules of the fluid are represented by mathematical particles, which we consider having the same size as the particles of the physical model (a). Each particle is characterized by its position $\vec{x}$ and its velocity $\vec{v}$. These particles are positioned in a simulation box (see Fig. 1(a)). Because of the use of periodic boundary conditions in the directions parallel to plates, this box represents the infinite physical system described above. The plates are modelled using thermal wall boundary conditions, implicating that particles that hit such a wall are reflected with a new velocity randomly chosen from a distribution corresponding to the temperature of that wall. According to [3], when a particle strikes a perfect thermal wall at temperature T_w, all three components of the velocity are reset according to a biased Maxwellian distribution. The component normal to the wall is distributed as $P_\perp(V_\perp) = \frac{m}{kT_w} V_\perp \mathrm{e}^{-mv_\perp^2/2kT_w}$, and each parallel component is distributed as $P_\parallel(V_\parallel) = \sqrt{(m/2\pi kT_w)}\,\mathrm{e}^{-mv_\parallel^2/2kT_w}$, where m is the particle's mass and k is Boltzmann's constant.

Due to their velocity the particles move through the flow field region and can thus collide with each other. Important of this method is that the particle trajectories are not used to calculate collisions with other particles explicitly. Instead, the method uses a computationally much cheaper approach, where collisions are performed stochastically. This is obtained using the following scheme. Repeatedly, the particles are first advected and subsequently collisions are calculated stochastically. In the advection step, the particles are moved according to their velocities and the time step size. During the collision step collision partners are selected from predescribed collision probabilities. This is done by dividing the system into cells. A particle in a given cell can collide with particles in nearby cells. The chance that two such particles really collide depends on their relative velocities and the binary collision integral $J_E(F,F)$. Whenever a collision is accepted the velocities are changed according to [7,8] ensuring the exact global conservation of momentum and energy.

Since the method is intrinsically designed to solve the unsteady Enskog equation, after preparing the particle system in a suitably chosen initial state, a number of time steps has to be computed until the transient dies out; then the sampling of the particle properties starts to be gathered and the time averaged macroscopic quantities are obtained.

2.4. Molecular dynamics

The second simulation method to simulate the channels is molecular dynamics (MD). In a MD simulation, the exact particle trajectories are calculated by computing all the forces that the particles exert upon each other. These forces are described by means of interaction potentials. A commonly used potential to describe the interactions between particles is the Lennard-Jones (LJ) potential

$$V_{\mathrm{LJ}}(r) = \epsilon\left[\left(\frac{2R_{\mathrm{vdW}}}{r}\right)^{12} - 2\left(\frac{2R_{\mathrm{vdW}}}{r}\right)^{6}\right], \tag{6}$$

where ϵ is the interaction strength and R_{vdW}, the van der Waals radius, a measure for the particle size. The LJ potential is mildly attractive as two molecules approach each other from a distance, but strongly repulsive when they come too close.

In order to simulate hard-sphere like interactions using MD, truncated shifted Lennard-Jones (tsLJ) potentials were used for the interactions between gas molecules. This potential is defined as

$$V_{\mathrm{tsLJ}} = \begin{cases} V_{\mathrm{LJ}}(r) - V_{\mathrm{LJ}}(r_c) & \text{if } r \leqslant r_c, \\ 0 & \text{if } r > r_c, \end{cases} \tag{7}$$

where r_c is the cut-off radius. With a cut-off radius $r_c = 2R_{vdW}$, this basically means that only the repelling part of the LJ potential is taken into account such that all the attractive interactions between particles situated at larger distances are ignored. The choice of ϵ determines how hard the particle are. This is demonstrated in Fig. 2, where the hard-sphere potential is compared with our potentials. For the tsLJ potential with $\epsilon = 1$ the particles are still relatively soft, i.e. the particles can partially overlap during a collision. When two particles come closer together than $2R_{vdW}$, they start to repel each other. When they come closer together, kinetic energy is converted to potential energy until all kinetic energy in the direction of the separation between the two particles has been converted. Then the two particles move away from each other, where the potential energy is converted back to kinetic energy. A second measure for the particle size is thus given by the minimal distance between the two particles during such a collision, which we will refer to as the collision diameter. This collision diameter will be different for every collision as the velocities of all particles are different, however on average this collision diameter will approximately equal that distance for which the pair interaction potential $V(r)$ equals one. As this minimum distance during a collision compares well to the size of the particles in the MC simulations we will use this collision diameter to fix the value for R_{vdW} in Eq. (7). Thus, for $\epsilon = 1$ the choice $2R_{vdW} = 2^{1/6}a$ results in particles with average collision diameter a. For a stronger tsLJ potential with $\epsilon = 1000$ an average collision diameter a is obtained with the choice $2R_{vdW} = 1.005a$. These particles are very close to hard spheres and thus hardly overlap, such that the van der Waals radius is only slightly larger than $a/2$.

Periodic boundary conditions are used again in the directions parallel to the plates. The plates can be modelled again using the same thermal wall boundary conditions as used for the MC simulations. However, with MD it is also possible to simulate the walls explicitly (see Fig. 1(b)). Namely, an advantage of the MD method is that it is not only suited for simulating gases and liquids but also for crystals. With the MD method it is thus possible to model the walls and thus also the interaction of the gas particles with these walls explicitly. When the walls are simulated explicitly, LJ potentials are used to simulate the interaction of the particles in these walls. For the interactions of the molecules in the solid, the standard LJ potential is used with $\epsilon = 6$ in order to keep the crystal structure of the solid intact and to prevent the wall particles to evaporate and to mix with the gas molecules. The interactions between the wall particles and the gas particles and between gas particles mutually are modelled by weaker Lennard-Jones potentials or by a truncated shifted Lennard-Jones potential.

Thus, in MD both explicit wall and boundary conditions can be used to model the plates. The advantage of the use of boundary conditions is that much less particles are needed in the simulation and that the MC and MD method can be compared more fair on the same basis. The advantage of the use of explicit walls is that the interaction with the wall, that can be crucial for the total behavior, can be simulated much more accurately. Being able to include a more accurate description of the interface is a very important feature of the hybrid method.

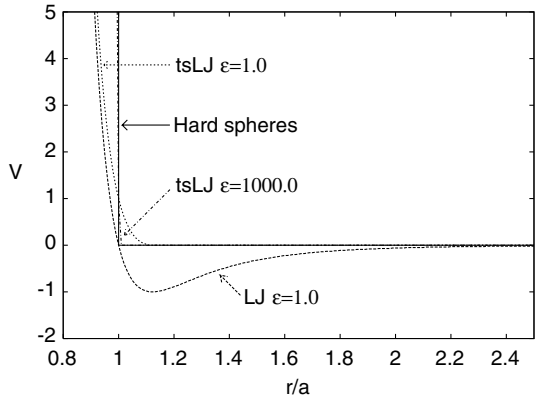

Fig. 2. Comparison of different potentials for the MD simulations. Shown are the Lennard-Jones potential (LJ), the truncated shifted Lennard-Jones potential (tsLJ) for two different values of epsilon and the hard-sphere potential.

Also from the MD simulations macroscopic properties can be derived, such as the density, the mean velocity, the temperature, the heat flux and the pressure.

2.5. Hybrid simulation molecular dynamics–Monte Carlo method

This simulation method combines the advantages of the molecular dynamics and Monte Carlo simulations [14], by simulating particles near the wall over the scale of the oscillation region using the molecular dynamics technique to obtain more accurate results near the wall, and Monte Carlo technique for the particles in the bulk to keep the computational cost as low as possible. This is achieved by dividing the simulation domain into subdomains, where either MD or MC is used. In order to get accurate results near the wall, a detailed model is needed in which the particles diameter in MC is equal to the molecular diameter of particles in MD, and three subdomains, two MD subdomains near the wall, and one MC domain in the middle of the channel.

An example of coupling two subdomains, one with MD and the other with MC is shown in Fig. 3. Because the MD method needs information from the neighboring MC particles and vice versa, an interface coupling the two subdomains is built as shown in the figure. The hybrid simulation method couples the MD and MC simulations through a buffer layer at the interface between the two domains. In Fig. 3 we have labeled with (II) the buffer layer of MC subdomain (III + IV), and with (III) the buffer layer of the MD subdomain (I + II).

Our simulation algorithm consists of the following steps:

1. Generate initial configuration, i.e. initial positions and velocities for all particles in the whole domain.
2. Assign particles in region I and II to MD code, and in III and IV to MC code.
3. Send properties of particles in region II to MC code, and of particles in region III to MD code.
4. MD simulations of particles in I, II, and copy of region III (BL_{MD}), and MC simulations in III, IV, and copy of region II(BL_{MC}) computing their new positions and velocities.
5. Start from step 3.

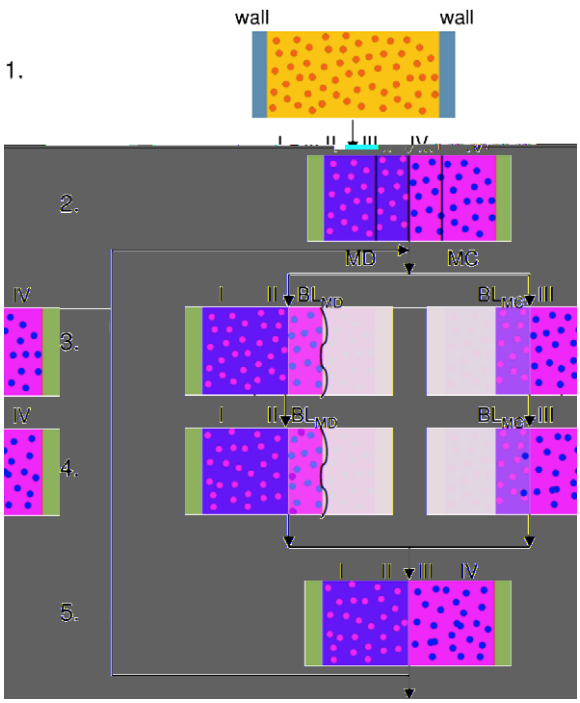

Fig. 3. The coupling of the MD and MC simulations is obtained via an interface layer.

Initially, the positions of the particles are randomly generated in the simulation domain, and the velocities of the particles are generated from a Maxwell–Boltzmann distribution. The particles in the region I and II in which MD is performed are send to the MD simulator and analogously the particles in the MC range (III and IV) are send to the MC simulator. As the MD simulation needs information from the neighboring MC particles and vice versa, this is obtained by creating an interface coupling the two subdomains. The MD simulation is extended with a buffer layer (BL_{MD}) to which the information of the MC particles in region III are copied and analogously the MC simulation is extended with a buffer layer (BL_{MC}) to which the information of the MD particles in region II are copied.

MC and MD simulations are updating then the velocities and positions of the particles assigned to their domain in parallel. As the time step size that can be made in one MD iteration is usually small compared to the time step size in MC, we have to do a number of MD time steps for every single MC simulation step. The information for the whole system is now obtained by recombining regions I and II from MD with regions III and IV from MC.

A straightforward approach to update particles in the interface layer ($BL_{MD} + BL_{MC}$) after each iteration, is by allowing each subdomain to communicate its own new particle positions and velocities to the other subdomain. In [9,14], we have investigated different coupling techniques between the two methods. Updating the interface can be realized by importing/exporting particles properties from one subdomain to another, or by considering the macroscopic properties in the interface region instead of single particles properties. Detailed explanations about updating the interface in the hybrid method is found in [14].

2.6. Comparison between MD and MC results – wall effects

In [9,14], we have compared the density profiles for a channel of width $L = 20\lambda$, when the temperature of the gas and of the wall is T, for a relatively dense hard-sphere gas ($\eta = 0.1$) using pure MC and pure MD simulations. First, we show that MD and MC yield comparable results when the same size of particles are used in the MD and MC simulations, and then we focussed on analyzing, where the differences between these results are.

In the MC simulations, one particle usually represents several gas molecules. We characterize thus first the influence of the particle size on the simulation profiles. Fig. 4 shows the density profiles for two systems with different particle size but with the same reduced density $\eta = 0.1$. From this figure, it is clear that for such high densities, the behavior is largely influenced by the particle size. Thus, for accurate simulations, at least near the wall, small particles are needed.

We characterize now the influence of different reduced densities and molecular sizes on our simulation results for the gas molecules in the micro and nano-channel. The density profiles in Fig. 4 are dependent on the particle size used for the simulations. The effect of the particle size on the simulation results is increasing

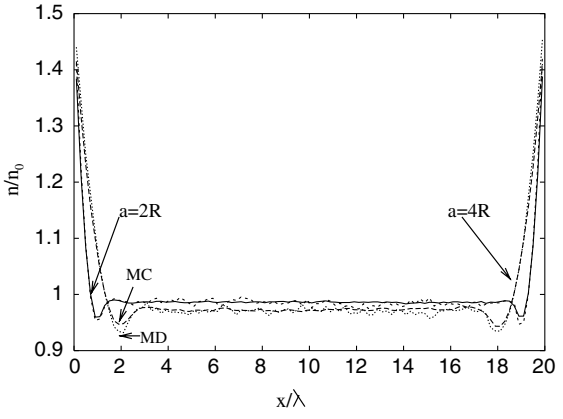

Fig. 4. Comparison between MD and MC density profiles n/n_0 for $\eta = 0.1$, $T = 1.0$, for two different particle sizes: $a = 2R$ and $a = 4R$.

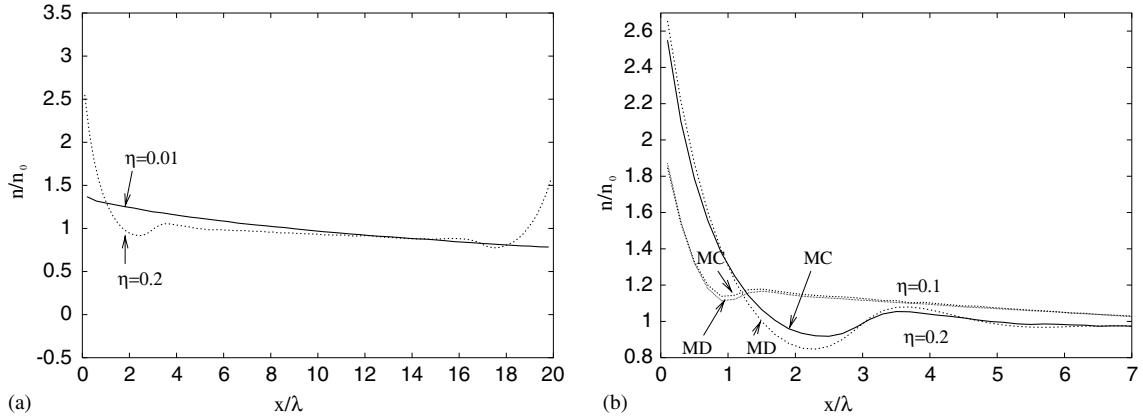

Fig. 5. (a) Comparison between MC density profiles n/n_0 for $\eta = 0.2$ and $\eta = 0.01$, in the presence of a heat flux ($T_2/T_1 = 2.0$). (b) Left part of the comparison between MD and MC density profiles n/n_0 for $\eta = 0.2$ and $\eta = 0.1$, in the presence of a heat flux ($T_2/T_1 = 2.0$).

with η and it is very small in case of a dilute gas (see Fig. 5(a)). When the same particle size is used in MC as in MD, we notice in Fig. 4 that the resulting density profiles are comparable. When the particle size is twice as large, we notice that the profiles are different near the boundary and in the middle as well (Fig. 4).

For dense gas oscillations appear near the walls. According to Frezzotti [7,8] this can be explained taking into account that when the distance of a molecule from the wall is less than the molecular diameter a, then a portion of its surface is protected from collisions since there is no room for a collision partner. The molecule is therefore pushed against the wall, which explains the high density of the molecules near the hard wall. The oscillatory density variations occur over a scale of the order of a. The number and the height of the peaks increase as the gas gets denser and denser. We show that these oscillations are the effect of crystallization near the hard walls as the densities become higher. At high densities particles are pushed against the wall and after the collision with the wall they can not be advected back into the channel because they are hindered by other particles. We have thus the so-called packing effect of the particles near the wall. We characterize these oscillations by studying the dependence of the position of these peaks and the height of these peaks on the system parameters.

We notice that pure MD and pure MC results are similar for relatively dense gases ($\eta = 0.1$), and differences appear in the peak region as an effect of the different collision mechanism. Even when we use the same particle size in MC as in MD (one molecule per simulated particle), ending in more expensive MC simulations, the MC and MD results are different, specially near the boundaries for large values of η (see Fig. 5(b)). These deviations between MC and MD increase in the peak region near the wall as η increases. Comparing Figs. 4 and 5, we notice that when a temperature gradient exists between walls, the MC and MD results still differ only in the oscillation region.

The real strength of the gas–gas interactions of the hard-sphere molecules modelled by tsLJ potential will not have much influence on the results but only on the computational time [8,9]. Anyway, we expect more differences to appear for a more detailed model, when explicitly including the walls within MD simulations. The pure MC is not good enough to describe micro and nano-channels accurately enough for the boundary properties. On the other hand, MD simulations can be very accurate but, to model a complete microchannel, MD simulations are too slow. We can thus apply the hybrid method by simulating MD near the wall in the oscillation region, for accurately simulating the wall effects, and MC in the bulk. For this we need to characterize how large is this oscillation region, and to study the dependence of the position and height of these peaks on the system parameters. For describing these properties, we introduce the following mathematical model.

3. The analytical model

For the calculation of the particles density and to study the density oscillations that appear near the wall we propose the following model. We consider the particles spheres with radius R (diameter $a = 2R$). They can

move along a line between 0 and L. This means that their centers can only move between R and $L - R$, and two neighboring particles cannot get closer to each other than a distance $2R$. The probability distribution of all particles is 0, where these restriction are violated and a constant c elsewhere (see Fig. 6). We are interested in the one-particle density.

3.1. The model with two particles

We look first at the model with just two particles. We derive the probability distribution of particle 1, P_1. This probability has the form:

$$P_1 = \int_{x_2 = x_1 + 2*R}^{L-R} c\,\mathrm{d}x_2 = c(L - 3R - x_1). \tag{8}$$

The probability distribution of particle 2 is

$$P_2 = \int_{x_1 = R}^{x_2 - 2R} c\,\mathrm{d}x_1 = c(x_2 - 3R). \tag{9}$$

The constant c can be determined by the condition that the first particle can be somewhere between R and $L - 3R$, $\int_{x_1=R}^{L-3R} P_1\,\mathrm{d}x_1 = 1$. From this equation, we find the constant c having the value:

$$c = 2\frac{1}{(4R - L)^2}. \tag{10}$$

We can now derive the one-particle density when there are just two particles ($P_{(2)}$):

$$P_{(2)} = \begin{cases} P_1 + P_2 = -c(-L + 6R), & 3R \leqslant x < L - 3R, \\ P_1 = c(L - 3R - x), & R < x < 3R. \end{cases} \tag{11}$$

So, in the middle of the pipe the probability of finding a particle is equally distributed between $3R$ and $L - 3R$. $P_{(2)}$ between R and $3R$ is equal to P_1 as it is not possible to have another particle there other than particle 1.

The plot of the left part of the particles distribution is in Fig. 7. We notice that in case of two particles we get only one maximum and that the curves switch at $x = 3$ in case $R = 1$.

For three and four particles the derivation is similar. For the one-particle density when there are three particles ($P_{(3)}$), we find:

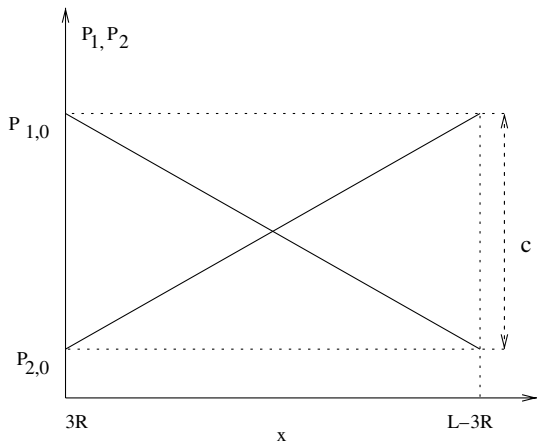

Fig. 6. Probability distribution of the particles between $3R$ and $L - 3R$, for the model with two particles. The sum $P_1 + P_2 = c$ for the middle of the channel.

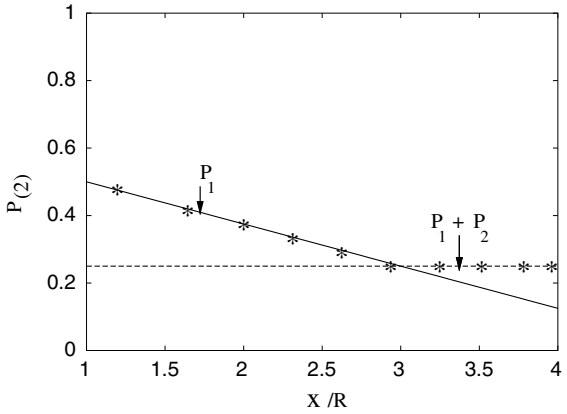

Fig. 7. Left part of the probability distributions, P_1, $P_1 + P_2$, when $R = 1$ and $L = 8R$. We have marked the $P_{(2)}$ between R and $3R(P_1)$, and between $3R$ and $L - 3R$ $(P_1 + P_2)$.

$$P_{(3)} = \begin{cases} P_1 + P_2 + P_3 = \frac{1}{2}c(L^2 - 16LR + 68R^2), & 5R \leqslant x < L - 5R, \\ P_1 + P_2 = \frac{1}{2}cx^2 + 5cRx + \frac{1}{2}c(L^2 - 16LR + 43R^2), & 3R \leqslant x < 5R, \\ P_1 = \frac{1}{2}c(-L + 5R + x_1)^2, & R \leqslant x < 3R. \end{cases} \tag{12}$$

In Fig. 8, we have the plot of $P_{(3)}$ for the case $R = 1$ and $L = 12R$. We notice that the curves switch at $x = 3$ and at $x = 5$, such that we have a maximum and then one minimum.

For the one-particle density when there are four particles in the channel $(P_{(4)})$ between R and $3R$, $3R$ and $5R$, $5R$ and $7R$, $7R$ and $L - 7R$:

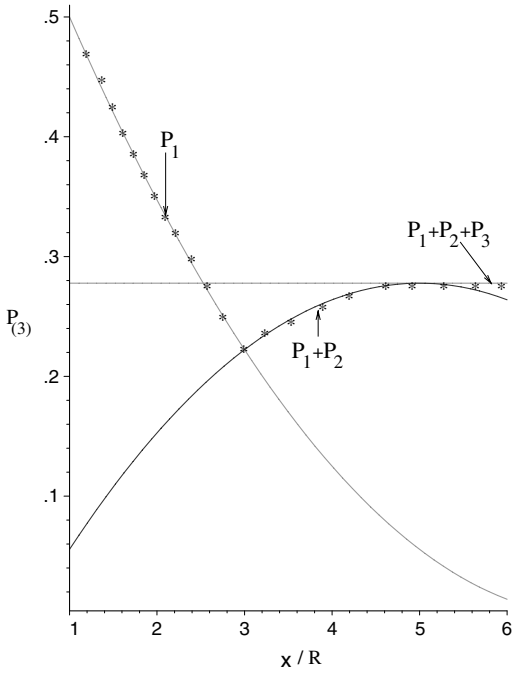

Fig. 8. Left part of the probability distributions, P_1, $P_1 + P_2$, $P_1 + P_2 + P_3$ when $R = 1$ and $L = 12R$. We have marked $P_{(3)}$ between R and $3R$, $3R$ and $5R$, $5R$ and $7R$, $7R$ and $L - 7R$.

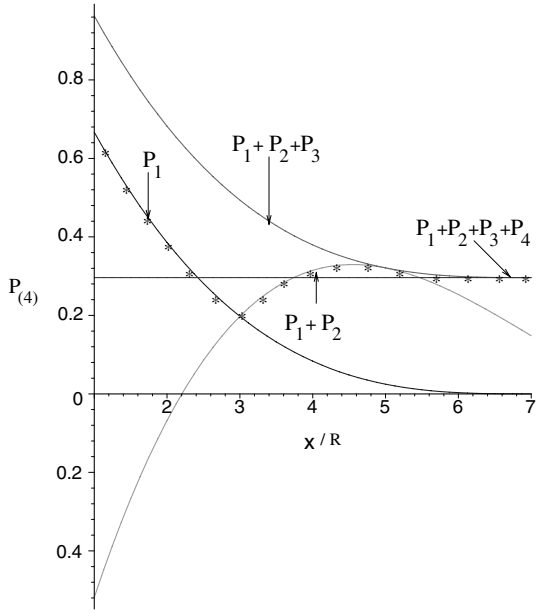

Fig. 9. Left part of the probability distributions, P_1, $P_1 + P_2$, $P_1 + P_2 + P_3$, $P_1 + P_2 + P_3 + P_4$, when $R = 1$ and $L = 14R$.

$$P_{(4)} = \begin{cases} P_1 + P_2 + P_3 + P_4 = -\frac{1}{6}c(30L^2R - 312LR^2 - L^3 + 1136R^3), & 7R \leqslant x < L - 7R, \\ P_1 + P_2 + P_3 = -\frac{1}{6}cx^3 + \frac{7}{2}cRx^2 - \frac{49}{2}cRx^2 - \frac{1}{6}c(30L^2R - 312LR^2 - L^3 + 793R^3), & 5R \leqslant x < 7R, \\ P_1 + P_2 = \frac{1}{3}cx^3 - \frac{1}{2}cLx^2 - cR(27R - 5L)x - \frac{1}{6}c(568R^3 - 237LR^2 + 30L^2R - L^3), & 3R \leqslant x < 5R, \\ P_1 = -\frac{1}{6}c(7R - L + x)^3, & R \leqslant x < 3R. \end{cases} \tag{13}$$

In Fig. 9, we have the plots of the one-particle distribution functions when $R = 1$ and $L = 14R$.

We notice that we get more and more maxima and minima when adding particles, which lead to the so-called oscillations near the wall.

3.2. Calculation of the particle density dependence

The dependence of the first maximum as a function of L and R for the model with two particles shows that this maximum at $x = R$ is decreasing with L and is increasing with R. For the case when $L = 20R$, we notice that the probability is increasing almost linearly with R for small values of R (Fig. 10). The value of the first maximum is decreasing with L as shown in Fig. 11.

3.2.1. The height of the oscillations peaks

In Figs. 12 and 13, we study how the height of the oscillation peaks depend on the system parameters like L, R and the number of particles. We notice that the height of these peaks is increasing with the number of particles, increasing with R and decreasing with L.

3.2.2. Position of the maxima and minima

For the model with three and four particles the position of the maxima and minima depends only on the radius of the particles. For four particles there is one maximum that slightly depends on L. The first minimum is in the region, where only one particle can come to the region where also the second particle can come. This point is at $3R$. The first maximum is, where the region begins, where also the third particle can come. This is at $5R$. Then there is a minimum at $7R$, which corresponds to the beginning of the region, where also a fourth

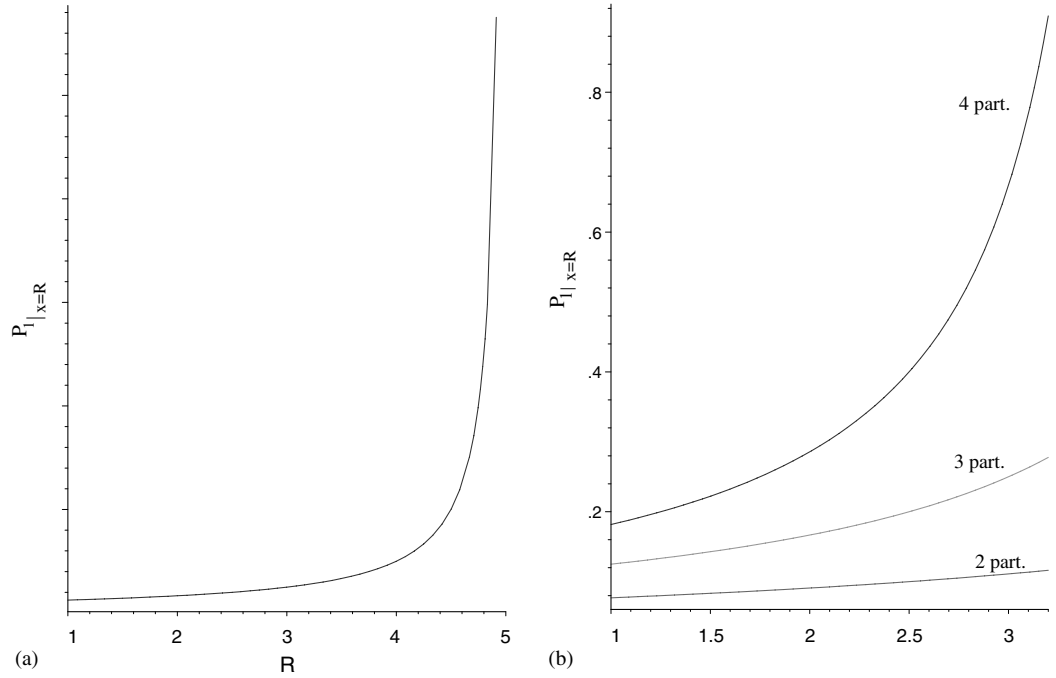

Fig. 10. (a) P_1 at $x = R$ as a function of R, when $L = 20R$. (b) P_1 at $x = R$ as a function of R when $L = 30R$, for the model with 2, 3 and 4 particles respectively.

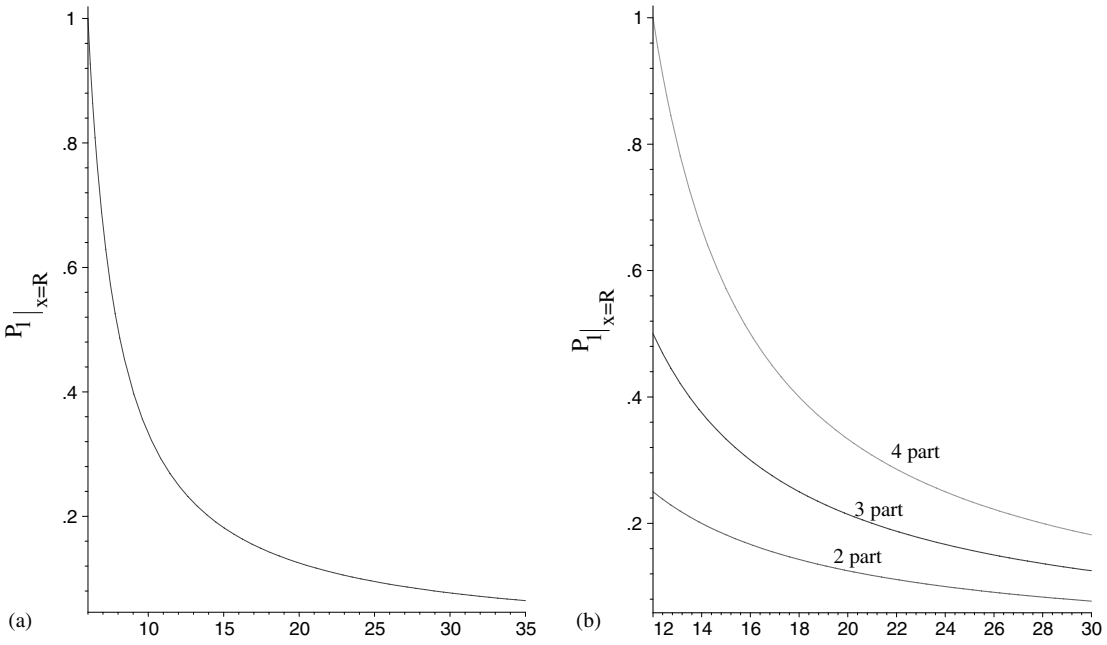

Fig. 11. (a) P_1 at $x = R$ as a function of L, when $R = 1$. (b) P_1 at $x = R$ as a function of L when $R = 1$, for the model with 2, 3 and 4 particles respectively.

particle can come. These minima and maxima are points, where the particle density gets a new contribution from an additional particle. For the 4-particle model we find one maximum just to the left at $5R$. Assuming $R \ll L$, the maximum is at $5R - 2R^2/L$, which means that there is a small L dependence.

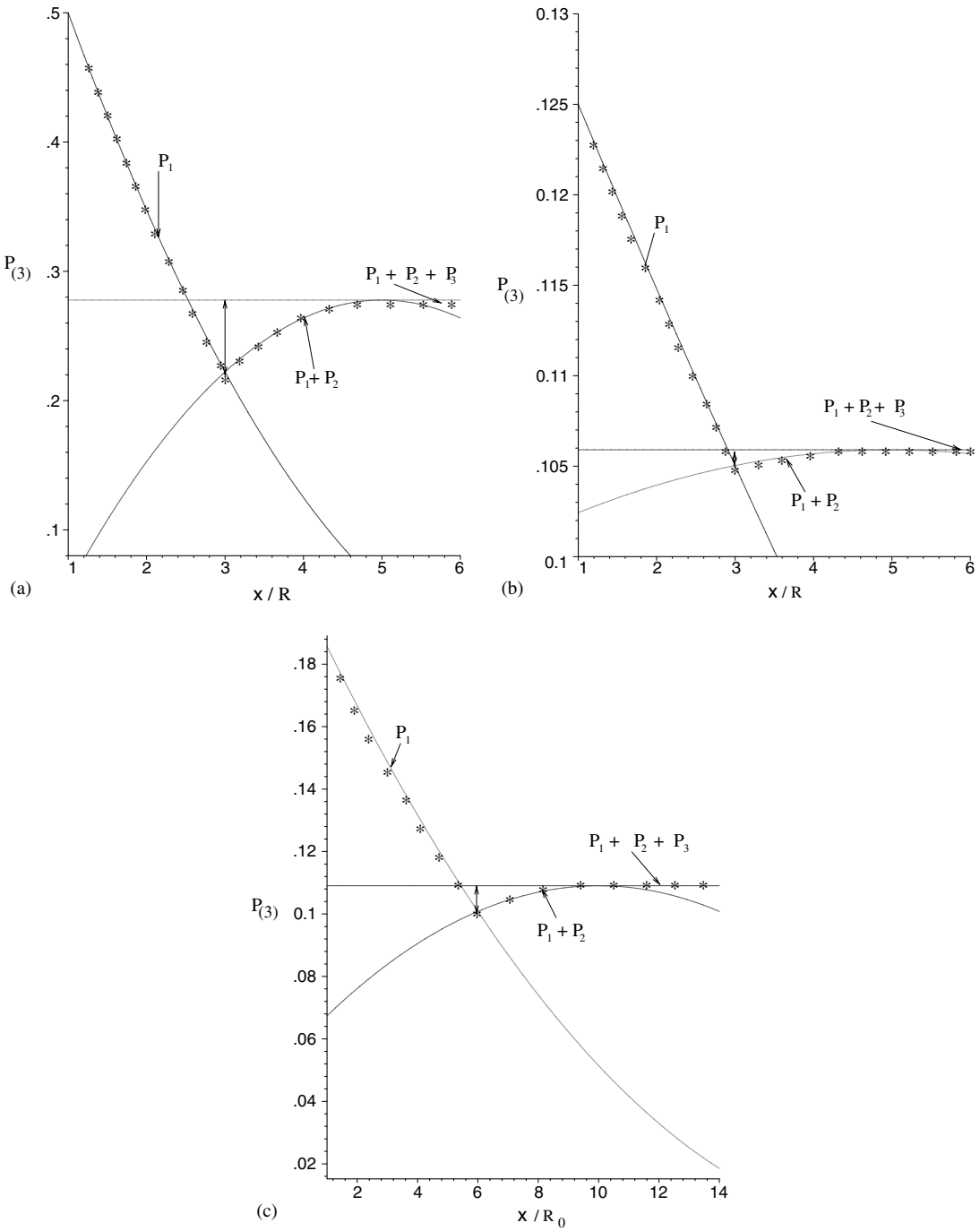

Fig. 12. (a) The left part of $P_{(3)}$ when $R = 1$ and $L = 12R$. (b) The left part of $P_{(3)}$ when $R = 1$ and $L = 30R$. (c) The left part of $P_{(3)}$ when $R = 2R_0$ and $L = 30R_0$, where the reference radius is $R_0 = 1$.

4. Analytical and simulation results

Our analytical model can explain the packing effect in a very qualitative way. In MC, increasing η the oscillations will increase. In our model, spherical molecules can move along a line between two walls that lead to oscillations of density near the walls. One might expect that when motion is added in the other two directions,

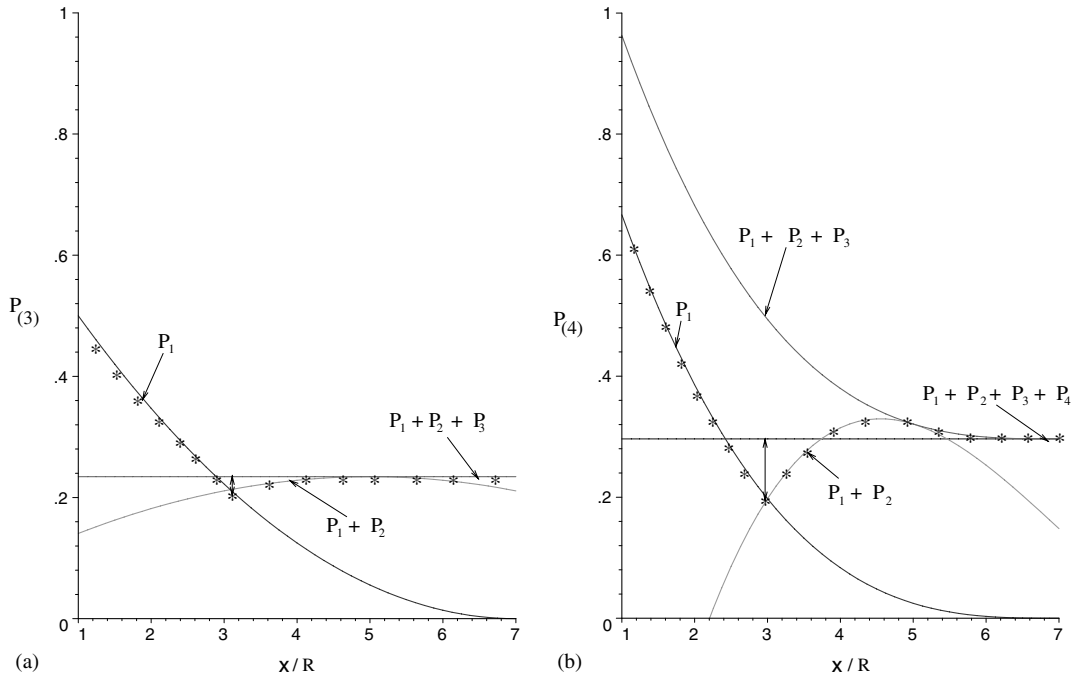

Fig. 13. Comparison between the peaks for the model with 3 and 4 particles: (a) Peaks for the model with 3 particles; (b) peaks for the model with 4 particles.

the oscillations will be masked, but this is not the case. MC simulations were done considering particles moving along a line in x direction and they were compared with MD simulations, where all the interactions were computed using LJ and truncated shifted LJ potential. The results of the simulations are similar disregarding the fluctuations. Therefore, we assume that our 1D model contains the origins of the oscillations.

In the MC, the computational costs can be reduced by concentrating the real molecules in large simulation particles. For a dilute gas this is the standard way of avoiding the simulation of all the molecules in the gas but for a dense gas this can lead to erroneous simulations. When we put two real molecules in one simulation particle, the diameter of these particles is twice as large as the one of a real molecule. We study the effect on the simulation results of increasing the size of the simulated particles. When increasing the size of the particles, the mean free path λ should be scaled also in order to have η constant. This is because η constant imply (λ/a) constant as $\frac{\lambda}{a} = \frac{(1-\eta)^3}{3\sqrt{2}\eta(2-\eta)}$. We look at the normalized number density n/n_0 for $R = 1,\ldots,5$ such that $\eta =$ constant. In Fig. 14, we have the simulation results for n/n_0 for molecules with different diameters, when $\eta = 0.1$. The peaks near the wall influence the results in the middle of the system such that the higher the deeps, the lower the normalized density in the middle. We study this error by plotting the dependence of $[1 - (n/n_0)]$ on system parameters. In order to make the results of the simulations independent of the particles used, we would like to have similar results for the normalized densities in the middle and only different in the oscillatory region. Depending on the system parameters used, this error can be smaller or larger. Thus, we can determine how large an error is for a certain mapping of real molecules into simulating particles (particle size).

From our MC results we see that the normalized density n/n_0 in the middle of the channel is increasing with L for $R =$ const. like in Fig. 15. For higher values of η, $[1 - n/n_0]$ is larger. In Fig. 15 we can see that for a dense gas $\eta = 0.2$, the effect of the boundary is larger for normalized density in the middle of the channel $[1 - n/n_0]$. This means that for η around 0.1 we can use smaller channels while for more dense gas we have to use larger channels in order to minimize the effect of the boundary.

In Fig. 16, we have the normalized densities in the middle of the channel as a function on R for different L, when $\eta =$ constant. We notice that in this case the normalized density is linearly decreasing with R and the slope of these lines is increasing with decreasing the width of the channel. From the simulations we notice that

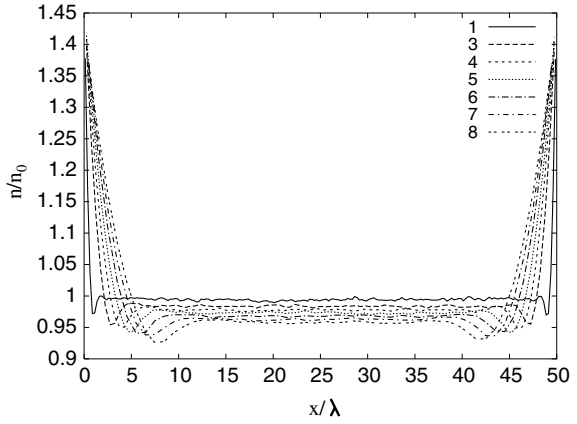

Fig. 14. Density profiles for $L = 50\lambda$ for $R = 1, 3, 4, 5, 6, 7, 8$, when $\eta = 0.1$.

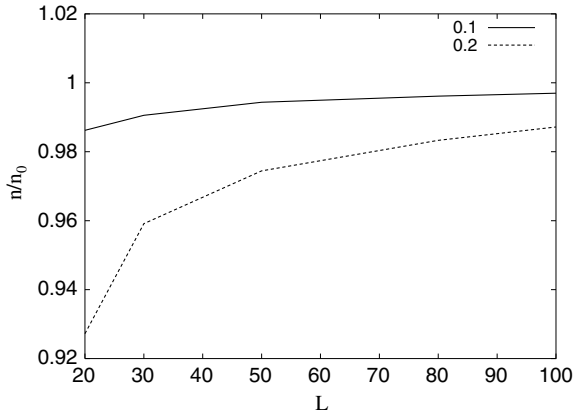

Fig. 15. Comparison between the normalized densities n/n_0 in the middle of the channel as a function on L for the case $R = 1$ when $\eta = 0.1$ and $\eta = 0.2$.

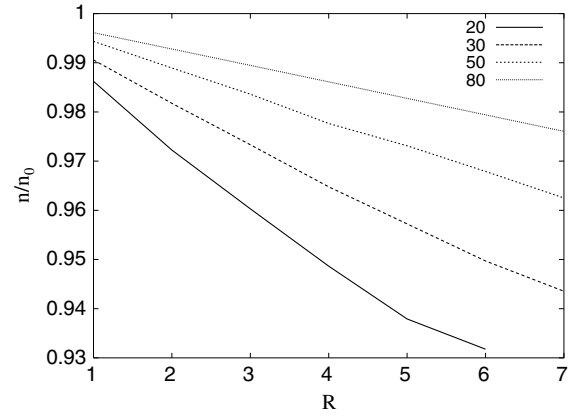

Fig. 16. Comparison between the normalized densities n/n_0 in the middle of the channel as a function on R for different width $L = 20R_0$, $30R_0$, $50R_0$, $80R_0$, where the reference radius is $R_0 = 1$.

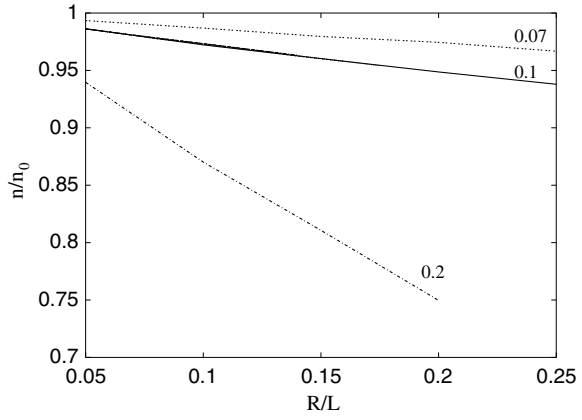

Fig. 17. The normalized densities n/n_0 in the middle of the system as a function on R/L for $\eta = 0.07$, 0.1, 0.2.

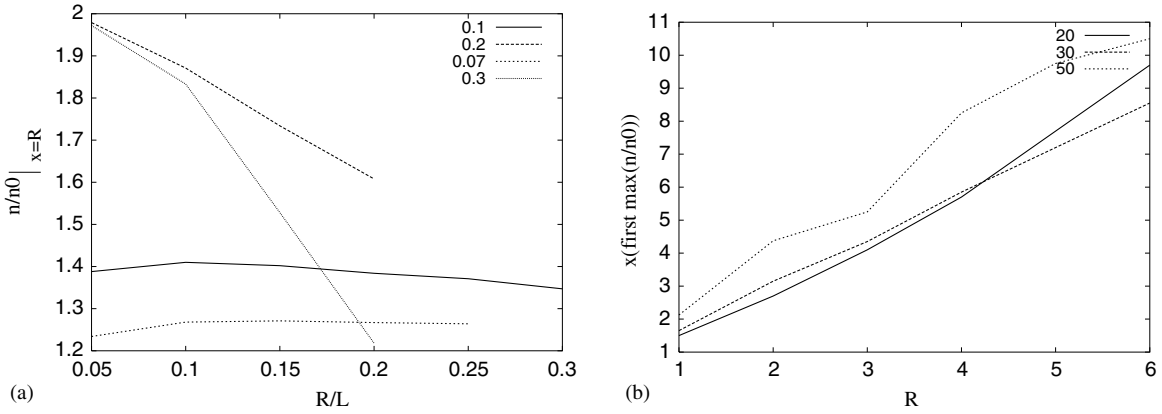

Fig. 18. (a) The first peak of the normalized densities n/n_0 near the wall of the channel as a function of R/L for $\eta = 0.07$, 0.1, 0.2, 0.3; (b) Comparison between the position as a function on R for different width $L = 20R_0$, $30R_0$, $50R_0$, where $R_0 = 1$.

the normalized density in the middle of the system depends actually only on the ratio between R and L. In Fig. 17, we see that the n/n_0 in the middle of the system is linearly decreasing with R/L, and the slope of these lines is dependent on η.

The normalized densities n/n_0 near the wall as a function on R/L for different η's show that this value is increasing with η (see Fig. 18(a)). For large values of R/L, n/n_0 is decreasing with R/L. At smaller η values ($\eta = 0.07$; $\eta = 0$, 1) we notice that for small values of R/L, n/n_0 is slightly increasing with R/L.

As illustrated in Fig. 18(b), the position of these peaks is only dependent on R.

5. Hybrid MC–MD simulation results

5.1. Deviations and wall effects of the hybrid simulation results for the number density

A new approach to have more accurate results and faster simulations is used to couple the two simulation methods using the hybrid MD–MC simulation method [9]. As described in the previous section, this approach is able to interplay between performing MD simulations near the solid walls and MC simulations for the bulk properties. The efficiency and accuracy of these simulations depend on the analysis of the dependence of the oscillation region on system parameters. We apply a hybrid simulation method, performing MD in the estimated oscillation region and MC for the bulk properties. We study the deviations from pure MD results of the hybrid simulation results, considering different lengths of the MD and MC simulation domains.

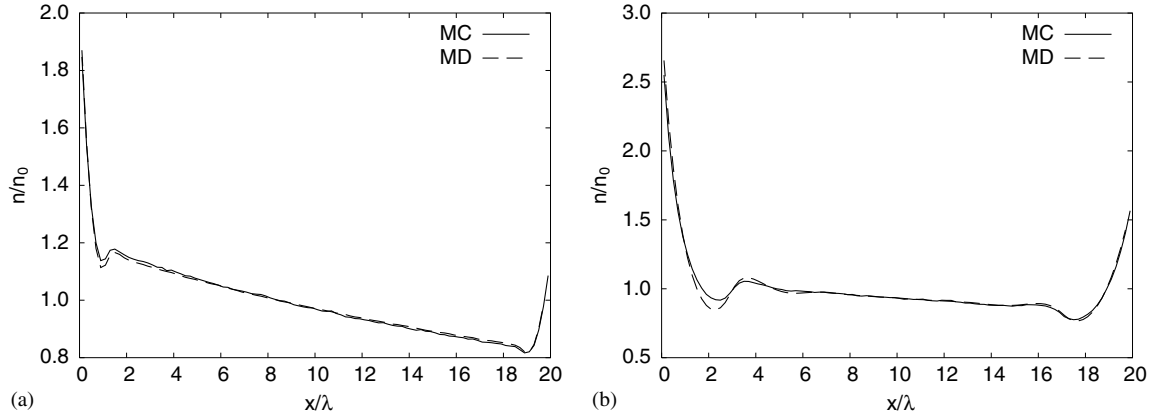

Fig. 19. Comparison of the deviations between the normalized density profiles (n/n_0) using the pure MD and pure MC, when (a) $\eta = 0.1$ and (b) $\eta = 0.2$.

As we can see from our previous analysis, for very small channels ($L = 20\lambda$) and relatively dense gas ($\eta = 0.2$) (see Fig. 17), the deviations are quite large, such that we choose to have 1 molecule per simulated particle within our MC simulations. From Fig. 18, we know that the position of these peaks is dependent only on R, such that this oscillation region will always be at a few molecular diameters next to the wall. For $\eta = 0.10$, the deviations in the simulation results are limited to the first oscillation peak. For $\eta = 0.2$, as the effect of the packing of molecules near the wall of the microchannel [7–9] determines the second layer of molecules to be formed near the wall, the oscillation region is extending and the deviations in this region increase compared to pure MD simulation results (see Fig. 19).

The previous analysis on the oscillation region helps on the optimal mapping of the particles to the MD and MC domains in the hybrid method according to the characteristic properties of the system. Thus, for small reduced densities η and small particle size (R) relative to width of the system L ($R \ll L$), the height of the oscillation peaks is slowly increasing with R/L, and for high densities is always decreasing with R/L. The position of these peaks depends only on the size of the particles when $R \ll L$ and it shows a small dependence on L for larger particles. In MC, the effect of increasing the particle size on the boundary results (large artificial particles) can be estimated. This effect is small for more dilute gases ($\eta = 0.07$) and when $R \ll L$ (see Fig. 21). More molecules per simulating particle can be used in this case. Deviations become significant as the effect of the boundary becomes important when increasing η and when using very large artificial particles. When $\eta \geqslant 0.2$, one molecule per particle should be used if $L \leqslant 100\ \lambda$. In case $L \geqslant 100$ we have small deviations (1–2%) between simulation results in the middle of the channel when using more molecules per particle. In the region next the wall, where the boundary effects are still important we apply a more accurate method as MD (see Fig. 20) and we couple it with MC in the middle of the channel. This will have a good effect for the deviations in the simulation results in the channel.

We quantify the deviations in the simulation results comparing with pure MD simulations results for the number density, when using pure MC and hybrid MC–MD simulation methods for different reduced densities ($\eta = 0.1$, and $\eta = 0.2$). The results show that efficiency and accuracy of these simulations depend on the size of the MC and MD domains. For the hybrid MC–MD simulations we determine then how large are these deviations when different sizes of the MD domain are used.

5.2. Simulation accuracy and efficiency

The deviations in the simulation results for the number density of a relatively dense gas using the hybrid MD–MC method, are smaller when compared to pure MD results than for the pure MC results, as we can see in Fig. 20. From Fig. 20, we see that hybrid simulations follow the MD simulations, while MC has large deviations. These deviations are increasing with η, and are decreasing when increasing the width of the MD

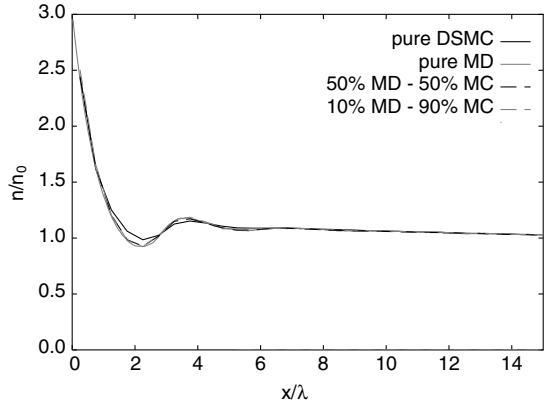

Fig. 20. Comparison between the normalized density profiles (n/n_0) near the left wall of the channel using the pure MD, pure MC, and hybrid MD–MC simulation methods for 10%MD–90%MC, and 50%MD–50%MC, when $\eta = 0.2$.

domain next to the wall in the hybrid method. In the hybrid MD–MC method, the accuracy of the results is determined by the lengths of the MD and MC domains, where the pure MD and pure MC are applied. For a dilute gas MC, MD and hybrid simulation profiles overlap. As we want to have the MD domain next to the wall, in order to have accurate results for the wall effects in the density profiles, we compare the simulation results using the hybrid method for different sizes of the domains. We notice that the most accurate results compared to pure MD density profile are the hybrid simulations for 50%MD–50%MC, while the pure MC have the largest deviations.

We compare again the density profiles simulation results for pure MD, pure MC, and hybrid MD–MC, this time for higher density, when $\eta = 0.2$ and $L = 50\lambda$. Zooming in the region next to the wall, we notice that the deviations of the pure MC compared to the pure MD results are increasing when increasing η to 0.2, but the hybrid simulations next to the wall still show very accurate results compared to the pure MD results (see Fig. 20). We notice that the deviations of the hybrid simulation method are decreasing when increasing the width of the MD domain next to the channel wall. For instance, when $\eta = 0.2$, the deviations of the hybrid simulation results for the case when we have 50% MD and 50% MC are around 0.246%, while for 10% MD and 90% MC are around 0.7%. We notice that the oscillations are increasing when decreasing the size of the MD domain, but even for the case of 10% MD domain, the deviations are almost 2.5 smaller than in the case of pure MC results.

For a very dilute gas, when $\eta = 0.001$, the pure MC, pure MD and hybrid MC–MD simulation results are in very good agreement and the deviations are negligible. In Fig. 21, we can see that the pure MC and pure MD results are just overlapping for the case of a very dilute gas.

We measure the accuracy of the simulation results for the number density n, by computing the deviations of the simulation results using the method mx from the pure MD simulation results that are considered to be the exact solution. The deviations are given by the relation $\sqrt{(n_{mx} - n_{\mathrm{MD}})^2}/n_{\mathrm{MD}}$, where n_{mx} stands for the density results when using the simulation method mx. The mx simulation method could be the MC, MD, or hybrid MD–MC with different sizes of the MD and MC domains.

The deviations in the hybrid simulation results are decreasing and are very small when increasing the width of the solid–gas interface. The deviations of the pure MC simulation results from the pure MD simulation results for the number density are found to be around 0.9%, when the reduced density $\eta = 0.1$ and the width of the channel $L = 50\lambda$. When the hybrid method is used, we noticed that the deviations are decreasing with a factor from two to three, and are between 0.32–0.42%. For more dense gas ($\eta = 0.2$), the deviations of the pure MC simulation results for the number density are found to be 1.71%, and the deviations of the hybrid MD–MC simulation results between 0.246% and 0.6977%.

The hybrid method is computationally less expensive than MD. For the coupled MD–MC simulations, two situations were considered. In the first case the simulation domain is equally divided between MD and MC. In the second case the MD domain covers only 10% of the whole domain corresponding to the oscillation region

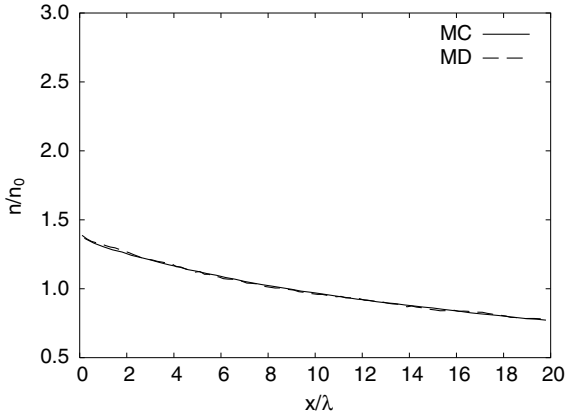

Fig. 21. Comparison between the normalized density profiles (n/n_0) using the pure MD and pure MC, when $\eta = 0.001$.

and 90% is the MC domain. The timing results presented in [9,14] show that the speedup when using hybrid MD–MC method for 50% MD and 50% MC is very small when compared to pure MD simulations times, but this speedup increases drastically when the bulk is larger than the region near the wall. For example, when the MC domain is extended to 90% of the simulation domain and MD domain reduced to 10% of the simulation domain, the speedup of the simulations increases roughly with a factor five. We notice also that this efficiency is independent of density [14].

6. Summary

We described how the density oscillations for a dense hard-sphere gas near the wall of a microchannel depend on the system properties such as density, width of the channel, and particle size. We built an analytical model that describes qualitatively the dependence of the oscillations on the system parameters. Comparisons between MD and MC simulation results for particles of different sizes are presented.

From the analytical model we notice that we get more and more maxima and minima when adding particles, which lead to the so-called density oscillations near the wall. The height of the density peak in the vicinity of the boundary is decreasing with L and increasing with R. When L is small, we notice that the probability is increasing almost linearly when R is much smaller than L ($R \ll L$). The height of the oscillation peaks is increasing with the number of particles, and is increasing with R/L. Position of the maxima and minima depends only on the size of the particles. Nevertheless, adding more particles we notice that there is one maximum that slightly depends on L.

These results are confirmed by the MC and MD simulation results. With the MC simulation results presented, the dependence of the oscillations peaks on system parameters is analyzed. From the MC simulations, for small reduced densities η and small particle size (R) relative to width of the system L ($R \ll L$), the height of the peaks is slowly increasing with R/L, and for high densities is always decreasing with R/L. The position of these peaks depends only on the size of the particles when $R \ll L$ and it shows a small dependence on L for larger particles. The effect of increasing the particle size on the boundary results (large artificial particles) can be estimated. We find that the effect is small for more dilute gases ($\eta = 0.07$) and when $R \ll L$. Deviations become significant as the effect of the boundary becomes important when increasing η and when using very large artificial particles. When $\eta \geqslant 0.2$ one molecule per particle should be used if $L \leqslant 100\lambda$. In case $L \geqslant 100$ we have small deviations (1–2%) between simulation results using more molecules per particle.

In the boundary layer, we studied also the deviations for the results of the properties of a hard-sphere gas near the walls of a micro/nano-channel using the hybrid MD–MC simulation method compared to the pure MD and MC results. When density is increased, the deviations in the pure MC results are increasing compared to pure MD results. The deviations in the hybrid simulation results are decreasing and are very small when increasing the width of the solid–gas interface. These deviations are smaller than the deviations of pure

MC simulation results, when compared to pure MD results, for any densities of the system. We have quantified these deviations of the simulations results compared to pure MD results for different reduced densities ($\eta = 0.1$, 0.2) and for different widths of the solid–gas interface. The deviations of the pure MC simulation results from the pure MD simulation results for the number density are found to be around 0.9%, when the reduced density $\eta = 0.1$ and the width of the channel $L = 50\lambda$, where λ is the mean free path. The reduced density is defined as $\eta = \pi n a^3/6$, where a is the molecular diameter. When the hybrid method is used, we noticed that the deviations are decreasing with a factor from two to three, and are between 0.32 and 0.42%. For more dense gas ($\eta = 0.2$), the deviations of the MC simulation results for the number density are found to be 1.71%, and the deviations of the hybrid MD–MC simulation results between 0.246% and 0.6977%. For more dilute gas, thus, no oscillation behavior next to the wall, the MC, MD and hybrid MC–MD simulations are in very good agreement and the deviations are negligible.

References

[1] F.J. Alexander, A.L. Garcia, B.J. Alder, A consistent Boltzmann algorithm, Phys. Rev. Lett. 74 (26) (1995) 5212–5215.
[2] F.J. Alexander, A.L. Garcia, B.J. Alder, The consistent Boltzmann algorithm for the van der Waals equation of state, Phys. A 240 (1997) 588–593.
[3] F.J. Alexander, A.L. Garcia, The direct simulation Monte Carlo method, Computer Simulation 11 (6) (1997) 196–201.
[4] G.A. Bird, Molecular Gas Dynamics and the Direct Simulations of Gas Flows, Clarendon Press, Oxford, 1994.
[5] D. Enskog, Kinetische Theorie der Waerme Leitung, Reibung and Selbstdiffusion in Gewissen Verdichten Gasen und Fluessigkeiten, Kungl. Svenska Veteenskapakad. Handl. 63 (1922) 3–44.
[6] D. Frenkel, B. Smit, Understanding Molecular Simulation, Academic Press, San Diego, 1996.
[7] A. Frezzotti, A particle scheme for the numerical solution of the Enskog equation, Phys. Fluids 9 (5) (1997) 1329–1335.
[8] A. Frezzotti, Monte Carlo simulation of the heat flow in a dense hard sphere gas, J. Mech. B/Fluids 18 (1999) 103–119.
[9] A.J.H. Frijns, S.V. Nedea, A.J. Markvoort, A.A. van Steenhoven, P.A.J. Hilbers, Molecular dynamics and Monte Carlo simulations for heat transfer in micro and nano-channels, in: Marian Bubak, G.Dick van Albada, Peter M.A. Sloot, Jack J. Dongarra (Eds.), Proceedings of the Workshop on Modelling and Simulation of Multi-Scale Systems, ICCS 2004, Part IV, Springer-Verlag, Berlin, 2004, pp. 666–671.
[10] A.L. Garcia, Numerical Methods for Physics, Prentice-Hall, Englewood Cliffs, NJ, 1994 (Chapter 10).
[11] J.M. Montanero, A. Santos, Monte Carlo simulation method for the Enskog equation, Phys. Rev. E 54 (1996) 438–444.
[12] J.M. Montanero, A. Santos, Simulation of the Enskog equation a la Bird, Phys. Fluids 9 (1997) 2057–2060.
[13] K. Nanbu, Theoretical basis of the direct simulation Monte Carlo method, in: V. Boffi, C. Cercignani (Eds.), Proceedings of the 15th International Symposium on Rarefied Gas Dynamics, Teubner, Stuttgart, 1986.
[14] S.V. Nedea, A.J. Markvoort, A.J.H. Frijns, A.A. van Steenhoven, P.A.J. Hilbers, Hybrid method coupling molecular dynamics and monte carlo simulations for properties of a hard-sphere gas in a micro-nano channel, Phys. Rev. E 72 (2005) 061705.
[15] P. Resibois, M. DeLeener, Classical Kinetic Theory of Fluids, Wiley, New York, 1977.
[16] N.F. Carnahan, K.E. Starling, Equation of state for nonatracting rigid spheres, J. Chem. Phys. 51 (1969) 635.
[17] C. Cercignani, Mathematical Methods in Kinetic Theory, Plenum Press, New York, 1990.
[18] S. Chapman, T.G. Cowling, The Mathematical Theory of Nonuniform Gases, Cambridge University Press, Cambridge, 1960.
[19] R.R. Schmidt, B.D. Notohardjono, High and server low temperature cooling, IBM J. Res. Dev. 46 (2002) 739–751.
[20] H. van Beijeren, M.H. Ernst, The modified Enskoq equation, Physica 68 (1973) 437–456.
[21] J. IsraelachviliIntermolecular Surface Forces, vol. 68, Academic Press, New York, 1991, pp. 437–456.